Journal of Materials Chemistry A

PAPER

View Article Online
View Journal | View Issue

Cite this: J. Mater. Chem. A, 2019, 7, 5712

A nitrogen-doped-carbon/ZnO modified Cu foam current collector for high-performance Li metal batteries†

Ying Zhou,[a] Kai Zhao,[a] Yu Han,[a] Zhenhe Sun,[a] Hongtao Zhang,[ab] Lingqun Xu,[a] Yanfeng Ma[ab] and Yongsheng Chen *[ab]

Received 14th December 2018
Accepted 8th February 2019

DOI: 10.1039/c8ta12064a

rsc.li/materials-a

The two most challenging issues for Li metal anodes are large volume change during the plating/stripping process and the growth of Li dendrites induced by uneven Li deposition. They lead to low coulombic efficiency, short cycling lifespan and serious safety issues of Li metal batteries. Here we developed a facile strategy to prepare a nitrogen-doped-carbon/ZnO (NDC/ZnO) modified Cu foam (MCuF) current collector for Li metal anodes. The MCuF shows stable Li plating/stripping behavior with the Li dendrite-mitigation feature. The resultant half cells achieve a super long lifespan of over 600 cycles at 1 mA cm^{-2} and over 200 cycles at a high current density 10 mA cm^{-2}. Moreover, the full cell paired with $LiFePO_4$ also exhibits a long lifespan of over 150 cycles at a high rate of 5C. Such high performance can be attributed to the characteristics of MCuF, including its 3D porous structure with high conductivity, enlarged surface area and uniform lithophilic NDC/ZnO sites. We believed that our work can provide a facile strategy for fabricating high-performance 3D current collectors for Li metal storage and stable Li metal batteries.

Introduction

The increasing demand for portable devices and electric vehicles has stimulated intensive studies focusing on high energy density batteries such as lithium–sulfur (Li–S) batteries and lithium–oxygen (Li–O_2) batteries.[1–3] Li metal is considered as a promising anode material for these high energy density batteries due to its extremely high capacity (3860 mA h g^{-1}) and the lowest negative electrochemical potential (−3.040 V *vs.* the standard hydrogen electrode).[4,5] However, the practical application of Li metal anodes is still restricted by several serious problems.[6] On the one hand, the volume change during the Li plating/stripping process results in the breaking of the SEI, leading to a short cycling lifespan due to the irreversible consumption of Li.[7] On the other hand, inhomogeneous Li deposition induces continuous growth of Li dendrites, which results in safety issues due to short circuiting, a low coulombic efficiency (CE) and a short lifespan.[8,9] Considerable efforts have been made to solve the above issues. To stabilize the SEI film of Li metal anodes, several approaches have been studied including (1) forming an *in situ* SEI *via* optimizing the electrolyte additives[10–13] and (2) constructing an *ex situ* SEI such as a physical protection layer[14,15] and artificial fast Li^+ conductors.[16–18] However, such SEI films still cannot bear the intrinsic volume change during the Li plating/stripping process. Many studies have been devoted to accommodating the volume change of Li *via* 3D host structures including 3D wood,[19,20] 3D polymer matrices,[21] 3D Ni foam,[7] 3D silver/graphene hosts[22] and reduced graphene oxide paper.[23] Moreover, the 3D hosts take advantage of their relatively large specific area which can reduce the effective current density.[4] However, their low conductivity, complicated preparation methods, high cost and/or nonuniform deposition of Li are still challenging issues. As a result, there is high demand for better methods to fabricate 3D porous hosts with high conductivity and uniform Li deposition.

One of the most important Li hosts, 3D Cu,[24–26] which is also an important electrode component as the current collector, has enormous influence on Li deposition behaviour. Compared with conventional 2D Cu foil current collectors, 3D Cu current collectors exhibit better performance due to their high conductivity, porous structure and relatively large specific area.[27–29] However, it still remains a challenge for bare 3D Cu current collectors to guide a more uniform Li deposition due to their weak interaction with Li.[30,31] It has been reported that nitrogen-doped-carbon (NDC) and metal oxides can serve as lithiophilic sites to guide the Li^+ flux and lead to a uniform Li deposition due to their favourable interaction with Li.[19,20,31,32] ZIF-8, one of the most important MOF materials, has been

[a]The Centre of Nanoscale Science and Technology, Key Laboratory of Functional Polymer Materials, Nankai University, Tianjin, 300071, China. E-mail: yschen99@nankai.edu.cn

[b]The National Institute for Advanced Materials, Nankai University, Tianjin 300071, China

† Electronic supplementary information (ESI) available. See DOI: 10.1039/c8ta12064a

proved to be an ideal precursor to obtain NDC and ZnO sites simultaneously,[33,34] which is expected to be able to modify 3D Cu to guide and smooth the Li deposition.

Herein, we developed a facile strategy to fabricate NDC/ZnO modified Cu foam (MCuF) as a multifunctional current collector for Li metal anodes using ZIF-8 as the precursor. The NDC/ZnO particles were coated on the 3D skeleton of Cu foam through a simple wet-coating method, which could reduce the effective current density due to an increased specific area. Besides, the uniform lithiophilic NDC/ZnO sites can guide the homogeneous distribution of the Li^+ flux. Moreover, the 3D porous structure provides space for the volume change during the Li plating/stripping process. As a result, the MCuF current collector displays stable Li plating/stripping behaviour with dendrite-migration properties. The resultant half cells achieve a super long lifespan of over 600 cycles at 1 mA cm^{-2} with a high CE of over 97.8% and relatively low overpotential. Even at a high current density of 10 mA cm^{-2}, they still show a high CE of 96.5% for over 200 cycles. Furthermore, full cells with the $LiFePO_4$ (LFP) cathode show the feasibility of the anode at a high rate.

Experimental section

Materials

The CuF was purchased from Saibo Electrochemical Material Co. It was washed with distilled water, alcohol and acetone successively before use. $Zn(NO_3)_2 \cdot 6H_2O$ was purchased from Aladdin Reagent Co. 2-Methylimidazole was purchased from Ark Pharm. The ZIF-8 was synthesized based on the process as described elsewhere.[35]

Preparation of MCuF

First, $Zn(NO_3)_2 \cdot 6H_2O$ (1.098 g) and 2-methylimidazole (2.433 g) were dissolved in 36 mL and 60 mL of methanol, respectively. Then, $Zn(NO_3)_2$ solution was added into the 2-methylimidazole solution to obtain a clear solution. A piece of CuF (40 mm × 40 mm) was immersed into the mixed solution. After stirring for 3 h, the ZIF-8 decorated CuF (CuF/ZIF-8) was obtained by picking the sheet out, washing with methanol three times and drying. The CuF/ZIF-8 was calcined at 600 °C for 3 h in an Ar atmosphere with a heating rate of 2 °C min^{-1}, which produced the final NDC/ZnO modified Cu foam (MCuF). The obtained MCuF was punched out into a disk with a diameter of 10 mm for further use.

Characterization

The morphological evolution of the electrode was characterized by using a Scanning Electron Microscope (SEM) (JEOL, JSM-7500F) equipped with an energy-dispersive X-ray spectrometry (EDS) system. The cycled electrode samples were finally disassembled from the cells, washed with dimethyl carbonate (DMC) to remove the residual electrolyte and then dried for 24 h for the SEM test. Transmission electron microscopy (TEM) was performed using a JEOL TEM-2100 electron microscope equipped with an energy-dispersive X-ray spectrometry (EDS) system. Powder X-ray diffraction (XRD) analysis was performed using an Ultima IV Rigaku diffractometer with Cu Kα radiation (data were collected at a scan rate of 10 degree min^{-1} in the range of 10–80°). X-ray photoelectron spectroscopy (XPS) was carried out using an AXIS HIS 165 spectrometer (Kratos Analytical) with a monochromatized Al Kα X-ray source (1486.71 eV photons) to analyze the chemical composition of the products.

Electrode fabrication and electrochemical measurements

Electrochemical measurements were carried out with coin-type cells. The half cells were assembled using CuF or MCuF as the working electrode and Li foil as the reference electrode. The symmetrical cells were assembled using CuF@Li or MCuF@Li as the working electrode and Li foil as the reference electrode. For this purpose, CuF@Li and MCuF@Li anodes were obtained by electrochemical preprocess. After plating 6 mA h cm^{-2} Li on CuF and MCuF, the CuF@Li and MCuF@Li electrodes were disassembled from half cells and reassembled into symmetrical cells. For the full cells, LFP was employed as the cathode. The LFP electrode was fabricated as follows: LFP powder was mixed with polyvinylidene fluoride (PVDF) and super-P at a weight ratio of 8 : 1 : 1. The obtained homogeneous slurry was casted on an Al current collector and then dried at 60 °C for 3 h and 150 °C for 1 h under vacuum. Then the obtained LFP sheets were pressed and punched into circular disks with diameters of 10 mm and the areal mass loading is ≈7.3 mg cm^{-2}, corresponding to a capacity loading of ≈1.2 mA h cm^{-2}. And the CuF@Li and MCuF@Li anodes were prepared using the same process as that of the symmetrical cells. For all the half cells and symmetrical cells, the electrolyte was 1 M LiTFSI in DOL/DME (volume ratio 1 : 1) with 1 wt% $LiNO_3$. For full cells, the electrolyte was 1 M LiTFSI in DOL/DME (volume ratio 1 : 1) with 2 wt% $LiNO_3$. A Celgard 2325 was used as the separator. All cells were assembled under argon conditions in a glovebox.

The electrochemical performance was measured with a two-electrode electrochemical cell by using an automatic battery tester system (Land CT2001A model, Wuhan LAND Electronics Ltd). In each galvanostatic cycle of half cells, a fixed amount of Li was deposited on the electrode at different current densities and then stripped away up to 1 V at the same current density.

Results and discussion

Fabrication and characterization of MCuF

The fabrication process of MCuF is shown in Fig. 1a, and the details are described in the Experimental section. Typically, a piece of CuF was immersed into the precursor solution of ZIF-8 consisting of $Zn(NO_3)_2$ and methylimidazole and then stirred for 3 h. The MCuF was facilely obtained by calcining the ZIF-8 decorated CuF (CuF/ZIF-8) at 600 °C in an Ar atmosphere. The low-magnification SEM images of CuF and MCuF and the optical photographs are shown in Fig. S1.† It is observed that the CuF (Fig. S1a†) exhibits a glossy orange color and the skeleton surface of its 3D structure is smooth with a pore size of 100–300 μm, but the obtained MCuF (Fig. S1b†) displays a uniform color of black and the 3D porous structure of CuF is

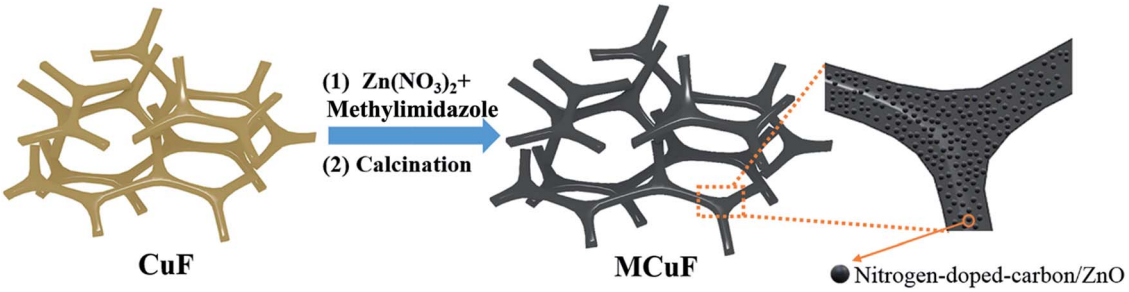

Fig. 1 Schematic illustration of the fabrication process of MCuF.

still maintained. Besides, the skeleton surface becomes rougher, proving the formation of a coating on CuF.

Fig. 2a shows the SEM images of MCuF (inset is the magnification of the selected area). It is observed that the surface coating layer consists of evenly distributed particles. Moreover, Fig. 2b shows the EDS mapping results of the same zone of Fig. 2a, and the evenly distributed C, N, Zn and O demonstrate the uniform distribution of the particles on the surface of MCuF.

Furthermore, the TEM image (Fig. S2a†) shows that the particle size is about 50 nm, and four elements of C, N, Zn and O are distributed in the particles uniformly (Fig. S2b–e†). XRD and XPS were also used to further characterize the chemical composition of MCuF. The XRD pattern of MCuF (Fig. 2c) shows the existence of the ZnO phase,[36] which originates from the CuF/ZIF-8 (Fig. S3†) after calcination.[37] Fig. S4† shows the XPS survey spectrum, four elements of C (61.2 at%), Zn (4.82 at%), O (10.24 at%) and N (21.7 at%) were also detected. The high-resolution Zn 2p spectrum (Fig. 2d) displays two peaks at about 1022 eV (Zn $2p_{3/2}$) and 1045 eV (Zn $2p_{1/2}$), respectively.[36] Moreover, the high-resolution O 1s spectrum (Fig. S5†) exhibits the existence of Zn–O,[38,39] which is consistence with the XRD result. Besides, the high-resolution N 1s spectrum (Fig. 2e) shows three fitted peaks at 398.7 eV, 400.8 eV and 403.4 eV, which can be assigned to pyridinic N, pyrrolic N, and graphitic N, respectively.[32,40] The XRD and XPS results further confirm that the four elements exist in the form of NDC and ZnO. The evenly distributed lithophilic NDC/ZnO sites are expected to play a critical role of guiding the uniform deposition of Li.[19,21,32,35] Based on the results above, the obtained MCuF affords the following advantages: (1) the high conductivity of the 3D channel facilitates fast electron transportation, (2) the porous structure provides space for the volume change during the Li plating/stripping process, (3) the coating consisting of evenly distributed nano-particles increases the specific area of CuF and reduces the effective current density, and (4) the uniform NDC/

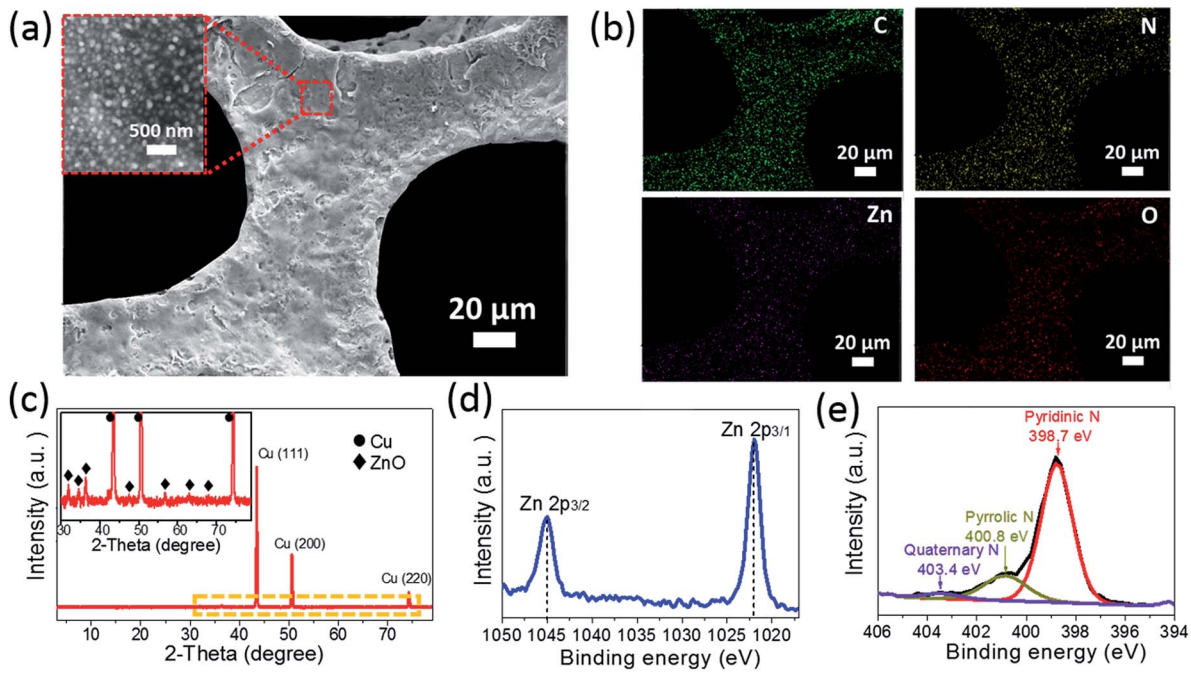

Fig. 2 Morphological and structural characterization of MCuF. (a) The SEM images of MCuF (inset is the magnification of the selected area). (b) The EDS results of the same zone of (a). (c) XRD pattern of MCuF (inset is the magnification of the selected area). (d) Zn 2p3 spectrum and (e) N 1s spectrum of MCuF.

ZnO lithophilic sites play a critical role of guiding the homogeneous distribution of the Li^+ flux. Therefore, the MCuF is believed to exhibit stable Li plating/stripping behaviour with the Li dendrite-mitigation feature.

Morphology of Li metal deposited on MCuF and CuF

To evaluate the Li storage performance of MCuF, the morphological evolution of Li metal plating on MCuF at a current density of 0.5 mA cm^{-2} was investigated by *ex situ* SEM (Fig. 3). Fig. 3a shows the morphology of MCuF before plating. After plating Li with an areal capacity of 1 mA h cm^{-2} (Fig. 3b), some small flower-like Li appears on the skeleton surface of MCuF without an obvious Li dendrite morphology. When plating up to 3 mA h cm^{-2} (Fig. 3c), the flower-like Li increase in size and grow close to each other without obvious growth of Li dendrites (inset is the magnification of Fig. 3c). Furthermore, when the Li metal is stripped off from MCuF by charging to 1 V (Fig. 3d), the surface retains almost its initial morphology, exhibiting the reversibility of Li and the structural stability of MCuF. For comparison, we also investigated the morphological change of bare CuF during Li deposition. Fig. 3e shows the morphology of CuF before plating. When plating Li with an areal capacity of 1 mA h cm^{-2} (Fig. 3f), some Li dendrites appear on the skeleton of CuF. When increasing the Li plating areal capacity to 3 mA h cm^{-2} (Fig. 3g), more large-size Li dendrites accumulate. Furthermore, when the Li metal is stripped from CuF (Fig. 3h), some Li dendrites still remain on the surface of CuF distributed unevenly, demonstrating the inactivation of some Li. Moreover, SEM images of MCuF and CuF after different cycles are shown in Fig. S6† to further characterise the morphological change of deposited Li. After the 10th plating at 1 mA cm^{-2} (Fig. S6a†), the deposited Li still exhibits the smooth morphology of MCuF, while some lumped Li deposits on the skeleton of CuF appear unevenly distributed (Fig. S6d†). Moreover, after the 10th plating (Fig. S6b†) and 50th plating (Fig. S6c†) at 3 mA cm^{-2}, the deposited Li on MCuF keeps a relatively smooth morphology with the dendrite-mitigation feature. However, the deposited Li on CuF is fragmentized (Fig. S6e and f†) under the same testing conditions, indicating the unstable deposition process using bare CuF. Such favourable behaviour of MCuF should be due to the following reasons. On the one hand, the MCuF guides a uniform Li^+ flux caused by the strong interaction between Li and lithophilic NDC/ZnO sites. On the other hand, the larger specific area than that of CuF attributed to the nano-particles reduces the effective current density, which is beneficial for suppressing the Li dendrite growth.

Electrochemical performance

To evaluate the performance of MCuF and better understand the role of NDC/ZnO modification, Li/MCuF half cells were assembled to measure the cycling stability and coulombic efficiency (CE). The Li/CuF half-cells were also assembled for comparison. Fig. 4a–d exhibit the CE results of CuF and MCuF at different current densities and cycling capacities. At a current density of 1 mA cm^{-2} with an areal capacity of 1 mA h cm^{-2} (Fig. 4a), MCuF shows stable performance with an average CE of 97.8% for over 600 cycles, while the CE of CuF oscillates up and down from the 40th cycle and drops to 72.6% after 380 cycles. At a higher current density of 3 mA cm^{-2} and 5 mA cm^{-2} shown in Fig. 4b and S7,† the MCuF still retains a high and stable average CE of 97.6% for over 400 cycles and 97.3% for 300 cycles, respectively. In comparison, the CE of CuF exhibits a fluctuant trend and rapidly decays after only 150 cycles and 120 cycles, respectively. Impressively, when increasing the current density to as high as 10 mA cm^{-2} (Fig. 4c), the MCuF can still remain a high average CE of 96.5% for a long lifespan of over 200 cycles, but the CuF exhibits a lower CE of about only 93.4% for 100 cycles, followed by a large fluctuation. When cycling at a current density of 3 mA cm^{-2} with a large areal capacity of 3 mA h cm^{-2} (Fig. 4d), MCuF still exhibits a high and stable CE of 97.2% over 120 cycles. In comparison, the CE of CuF exhibits a large

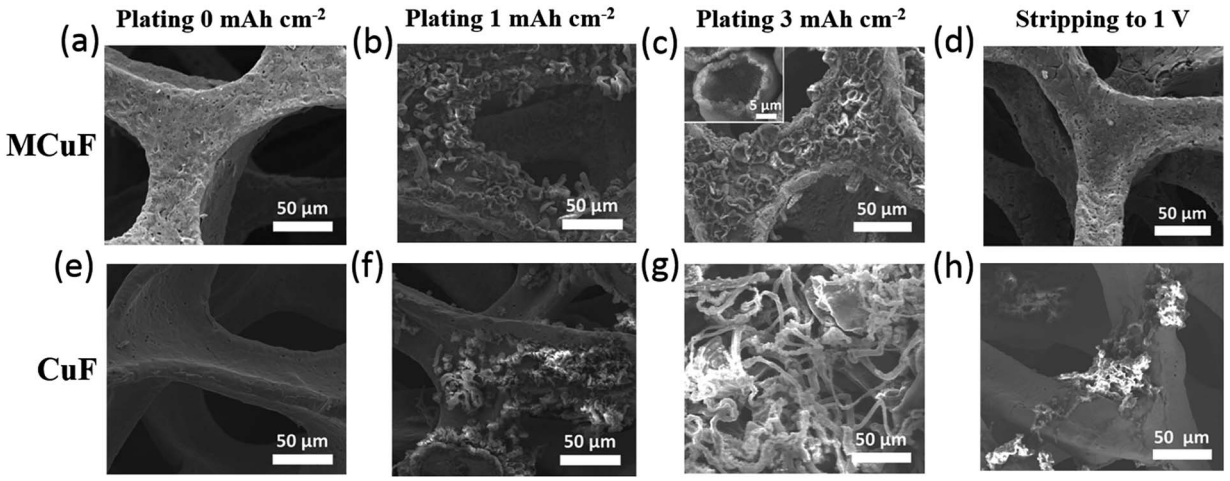

Fig. 3 Morphological evolution of Li plating on MCuF including (a) pristine MCuF and after plating at (b) 1 mA h cm^{-2} and (c) 3 mA h cm^{-2} and (d) after stripping to 1 V. Morphological evolution of Li plating on CuF including (e) pristine CuF and after plating at (f) 1 mA h cm^{-2} and (g) 3 mA h cm^{-2}, and (h) after stripping to 1 V.

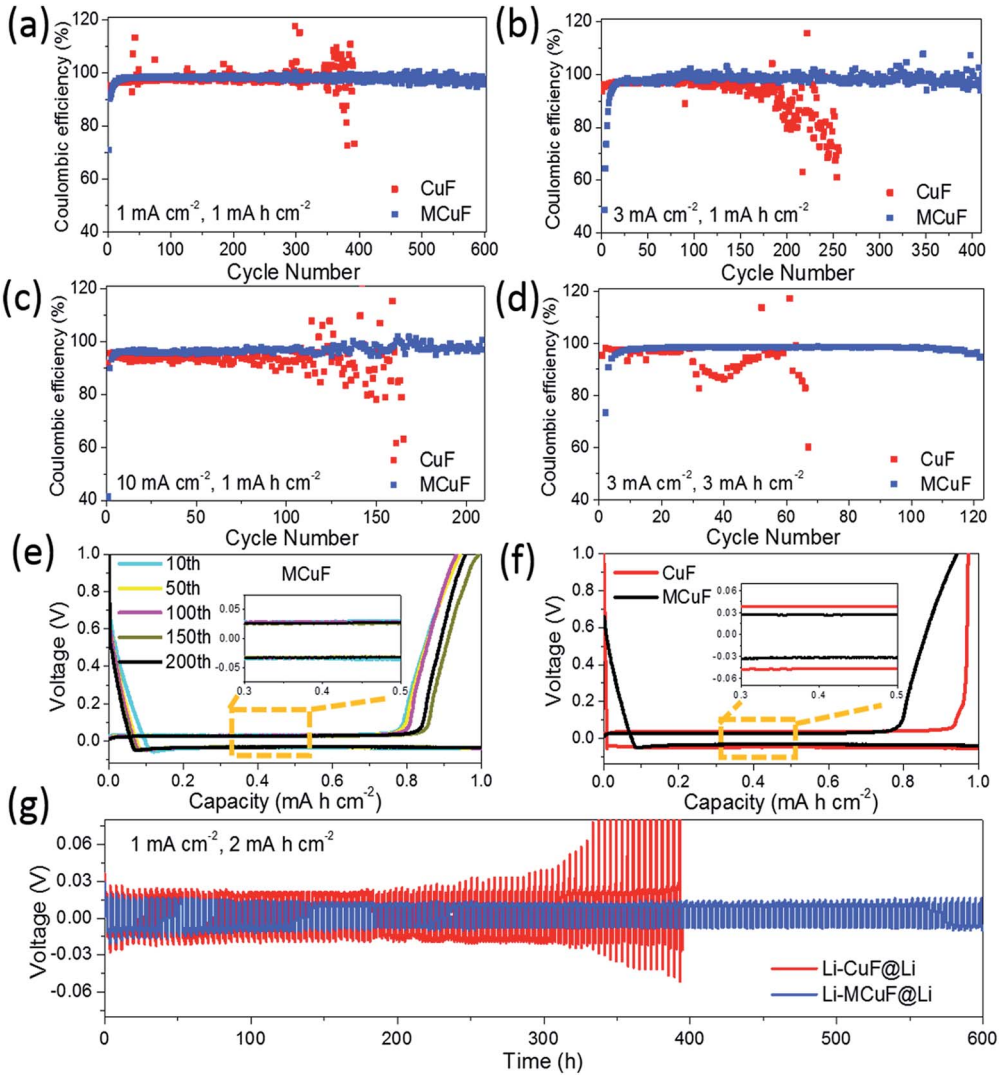

Fig. 4 Coulombic efficiency of Li plating/stripping on/from MCuF (blue) and CuF (red) at a current density of (a) 1 mA cm^{-2}, (b) 3 mA cm^{-2}, and (c) 10 mA cm^{-2} with an areal capacity of 1 mA h cm^{-2}. (d) Coulombic efficiency of Li plating/stripping on/from MCuF and CuF at a current density of 3 mA cm^{-2} with an areal capacity of 3 mA h cm^{-2}. (e) Voltage profiles of Li plating/stripping on MCuF at a current density of 3 mA cm^{-2} with an areal capacity of 1 mA h cm^{-2}. (f) Voltage profiles of Li plating/stripping on MCuF and CuF at a current density of 3 mA cm^{-2} with an areal capacity of 1 mA h cm^{-2}. (g) Voltage–time profiles of MCuF@Li and CuF@Li symmetrical cells at a current density of 1 mA cm^{-2} with an areal capacity of 2 mA h cm^{-2}.

fluctuation only after 13 cycles. These results demonstrate the higher and more stable behaviour of CE for MCuF than CuF, proving that the Li deposition is more uniform and the irreversible consumption of Li is suppressed using MCuF.[31] For further comparison, the long-term cycling performances of Cu-based current collectors in previous reports are listed in Table S1.† It is found that our MCuF current collector shows the best overall performance in consideration of the current density, areal capacity and cycling lifespan. To the best of our knowledge, long-term cycling at a current density as high as 10 mA cm^{-2} has never been reported in other reported Cu-based current collectors.

Fig. 4e shows the voltage profiles of Li plating/stripping on MCuF in the 10th, 50th, 100th, and 200th cycles at a high current density of 3 mA cm^{-2} with an areal capacity of 1 mA h cm^{-2}. The almost overlapping profiles indicate its stable Li plating/stripping behaviour. Besides, at 1 mA cm^{-2} (Fig. S8†), the MCuF electrode presents a low voltage hysteresis of ≈27 mV, while the voltage hysteresis of CuF is much higher (≈38 mV). Moreover, the MCuF still keeps a low voltage hysteresis of ≈60 mV with the current density increasing to 3 mA cm^{-2} (Fig. 4f), while the CuF presents a much higher voltage hysteresis of ≈85 mV. The smaller voltage hysteresis of MCuF is ascribed to its fast kinetics of Li^+ migration and superior interfacial properties.

Symmetrical cells were also fabricated to investigate the galvanostatic cycling performance of MCuF and CuF during plating/stripping processes. Fig. 4g and S9† show the voltage profile comparison of MCuF@Li and CuF@Li-based symmetrical cells at a current density of 1 mA cm^{-2} and 3 mA cm^{-2},

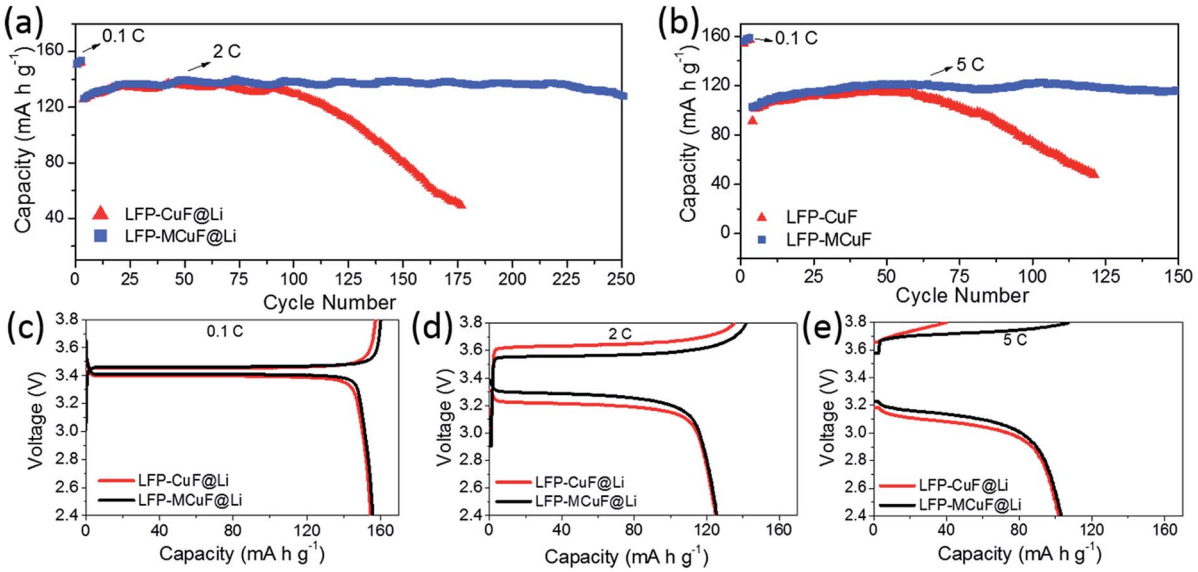

Fig. 5 Cycling performance of MCuF@Li-LFP (blue) and CuF@Li-LFP (red) full cells at (a) 2C and (b) 5C. Typical galvanostatic profiles of MCuF@Li-LFP (black) and CuF@Li-LFP (red) full cells at different current rates of (c) 0.1C, (d) 2C, and (e) 5C.

respectively, with a large areal capacity of 2 mA h cm^{-2}. At a current density of 1 mA cm^{-2} (Fig. 4g), the MCuF@Li symmetrical cell presents a stable voltage profile with a small overpotential of ≈11 mV for over 600 h, while the CuF@Li symmetrical cell exhibits a higher overpotential of 22 mV in the early cycling, which increases abruptly only after 200 h. When increasing the current density to 3 mA cm^{-2} (Fig. S9†), the MCuF@Li symmetrical cell still displays a long lifespan of over 300 h with a small overpotential of ≈18 mV. By comparison, the overpotential of the CuF@Li symmetrical cell continuously increases only after 75 h and the cell fails after about 150 h. These data reflect a much better electrode stability and transfer kinetics of the MCuF@Li symmetrical cell than that of CuF@Li.

To further explore the potential of the MCuF@Li electrode in a practical battery system, full cells were assembled by pairing LFP as the cathode as shown in Fig. 5. Meanwhile, LFP-CuF@Li full cells were also assembled for comparison. The areal mass loading of the LFP cathode is ≈7.3 mg cm^{-2}, corresponding to a capacity loading of ≈1.2 mA h cm^{-2}. Three cycles at 0.1C were conducted for initial activation before long-term cycling. As shown in Fig. 5a, the LFP-CuF@Li full cell displays a sudden capacity drop after 100 cycles at 2C, while the LFP-MCuF@Li full cell shows a better cycling stability of over 250 cycles. Moreover, the LFP-MCuF@Li full cell shows a favourable cycling stability for over 150 cycles even at a high rate of 5C, while the LFP-CuF@Li full cell displays a capacity drop after only 60 cycles. These data reveal a high Li reversibility in the MCuF-based full cell. Fig. 5c–e show the typical galvanostatic discharge/charge voltage profiles of the full cells at 0.1C, 2C and 5C, respectively. The MCuF-based full cells display lower voltage polarization than that of CuF at the different rates, indicating reduced effective current density and significantly improved kinetics.

Conclusions

In conclusion, NDC/ZnO modified Cu foam (MCuF) was developed by a facile strategy as a current collector for Li metal anodes. Based on the characteristics of MCuF such as its porous 3D structure, enlarged surface area and evenly distributed NDC/ZnO sites with lithiophilicity, the MCuF current collector guides a uniform Li deposition with the dendrite-mitigation feature. The resultant cells show a super long lifespan of over 600 cycles at 1 mA cm^{-2} and over 200 cycles at a high current density of 10 mA cm^{-2}, which has never been achieved in previous reports of Cu-based current collectors. We believed that our work can offer a competitive strategy to fabricate a high-performance current collector for Li metal anodes. Moreover, it sheds light on the design of high rate energy storage devices and promote the practical application of Li metal batteries.

Conflicts of interest

There are no conflicts to declare.

Acknowledgements

The authors gratefully acknowledge the financial support from the Ministry of Science and Technology of China (MoST, 2016YFA0200200), the National Natural Science Foundation of China (NSFC, 21421001, 51633002 and 51472124), Tianjin City (16ZXCLGX00100) and the 111 Project (B12015).

Notes and references

1 X.-B. Cheng, R. Zhang, C.-Z. Zhao and Q. Zhang, *Chem. Rev.*, 2017, **117**, 10403–10473.

2 X. Yang, L. Zhang, F. Zhang, Y. Huang and Y. Chen, *ACS Nano*, 2014, **8**, 5208–5215.
3 R. Fang, S. Zhao, Z. Sun, D. W. Wang, H. M. Cheng and F. Li, *Adv. Mater.*, 2017, **29**, 1606823.
4 Y. Guo, H. Li and T. Zhai, *Adv. Mater.*, 2017, **29**, 1700007.
5 J. M. Tarascon and M. Armand, *Nature*, 2001, **414**, 359–367.
6 H. Li and X. Xu, *Energy Storage Sci. Technol.*, 2016, **5**, 607–614.
7 S. S. Chi, Y. Liu, W. L. Song, L. Z. Fan and Q. Zhang, *Adv. Funct. Mater.*, 2017, **27**, 1700348.
8 G. Bieker, M. Winter and P. Bieker, *Phys. Chem. Chem. Phys.*, 2015, **17**, 8670–8679.
9 D. Lin, Y. Liu and Y. Cui, *Nat. Nanotechnol.*, 2017, **12**, 194–206.
10 W. Li, H. Yao, K. Yan, G. Zheng, Z. Liang, Y. M. Chiang and Y. Cui, *Nat. Commun.*, 2015, **6**, 7436.
11 S. Xiong, K. Xie, Y. Diao and X. Hong, *J. Power Sources*, 2014, **246**, 840–845.
12 R. Mogi, M. Inaba, S.-K. Jeong, Y. Iriyama, T. Abe and Z. Ogumi, *J. Electrochem. Soc.*, 2002, **149**, A1578–A1583.
13 F. Ding, W. Xu, G. L. Graff, J. Zhang, M. L. Sushko, X. Chen, Y. Shao, M. H. Engelhard, Z. Nie, J. Xiao, X. Liu, P. V. Sushko, J. Liu and J. G. Zhang, *J. Am. Chem. Soc.*, 2013, **135**, 4450–4456.
14 K. Yan, H. W. Lee, T. Gao, G. Zheng, H. Yao, H. Wang, Z. Lu, Y. Zhou, Z. Liang, Z. Liu, S. Chu and Y. Cui, *Nano Lett.*, 2014, **14**, 6016–6022.
15 K. Liu, A. Pei, H. R. Lee, B. Kong, N. Liu, D. Lin, Y. Liu, C. Liu, P. C. Hsu, Z. Bao and Y. Cui, *J. Am. Chem. Soc.*, 2017, **139**, 4815–4820.
16 L. Wang, Q. Wang, W. Jia, S. Chen, P. Gao and J. Li, *J. Power Sources*, 2017, **342**, 175–182.
17 Y. Liu, D. Lin, P. Y. Yuen, K. Liu, J. Xie, R. H. Dauskardt and Y. Cui, *Adv. Mater.*, 2017, **29**, 1605531.
18 D. Lin, Y. Liu, W. Chen, G. Zhou, K. Liu, B. Dunn and Y. Cui, *Nano Lett.*, 2017, **17**, 3731–3737.
19 Y. Zhang, W. Luo, C. Wang, Y. Li, C. Chen, J. Song, J. Dai, E. M. Hitz, S. Xu and C. Yang, *Proc. Natl. Acad. Sci. U. S. A.*, 2017, **114**, 3584–3589.
20 C. Jin, O. Sheng, Y. Lu, J. Luo, H. Yuan, W. Zhang, H. Huang, Y. Gan, Y. Xia and C. Liang, *Nano Energy*, 2018, **45**, 203–209.
21 Y. Liu, D. Lin, Z. Liang, J. Zhao, K. Yan and Y. Cui, *Nat. Commun.*, 2016, **7**, 10992.
22 P. Xue, S. Liu, X. Shi, C. Sun, C. Lai, Y. Zhou, D. Sui, Y. Chen and J. Liang, *Adv. Mater.*, 2018, **30**, e1804165.
23 D. Lin, Y. Liu, Z. Liang, H. W. Lee, J. Sun, H. Wang, K. Yan, J. Xie and Y. Cui, *Nat. Nanotechnol.*, 2016, **11**, 626.
24 C. P. Yang, Y. X. Yin, S. F. Zhang, N. W. Li and Y. G. Guo, *Nat. Commun.*, 2015, **6**, 8058.
25 L. L. Lu, J. Ge, J. N. Yang, S. M. Chen, H. B. Yao, F. Zhou and S. H. Yu, *Nano Lett.*, 2016, **16**, 4431–4437.
26 H. Zhao, D. Lei, Y.-B. He, Y. Yuan, Q. Yun, B. Ni, W. Lv, B. Li, Q.-H. Yang, F. Kang and J. Lu, *Adv. Energy Mater.*, 2018, **8**, 1800266.
27 S. H. Wang, Y. X. Yin, T. T. Zuo, W. Dong, J. Y. Li, J. L. Shi, C. H. Zhang, N. W. Li, C. J. Li and Y. G. Guo, *Adv. Mater.*, 2017, **29**, 1703729.
28 Y. An, H. Fei, G. Zeng, X. Xu, L. Ci, B. Xi, S. Xiong, J. Feng and Y. Qian, *Nano Energy*, 2018, **47**, 503–511.
29 Q. Yun, Y. B. He, W. Lv, Y. Zhao, B. Li, F. Kang and Q. H. Yang, *Adv. Mater.*, 2016, **28**, 6932–6939.
30 C. Zhang, W. Lv, G. Zhou, Z. Huang, Y. Zhang, R. Lyu, H. Wu, Q. Yun, F. Kang and Q.-H. Yang, *Adv. Energy Mater.*, 2018, **8**, 1703404.
31 R. Zhang, S. Wen, N. Wang, K. Qin, E. Liu, C. Shi and N. Zhao, *Adv. Energy Mater.*, 2018, **8**, 1800914.
32 L. Liu, Y. X. Yin, J. Y. Li, S. H. Wang, Y. G. Guo and L. J. Wan, *Adv. Mater.*, 2018, **30**, 1706216.
33 Y. Zhang, B. Lin, J. Wang, J. Tian, Y. Sun, X. Zhang and H. Yang, *J. Mater. Chem. A*, 2016, **4**, 10282–10293.
34 T. Kim, H. Kim, J.-M. Han and J. Kim, *Electrochim. Acta*, 2017, **253**, 190–199.
35 J. Wei, Y. Hu, Y. Liang, B. Kong, J. Zhang, J. Song, Q. Bao, G. P. Simon, S. P. Jiang and H. Wang, *Adv. Funct. Mater.*, 2015, **25**, 5768–5777.
36 F. Yin, Z. Zhang, Y. Zhang, C. Zhang and L. Xu, *Electrochim. Acta*, 2018, **270**, 274–283.
37 L. Wang, X. Zhu, Y. Guan, J. Zhang, F. Ai, W. Zhang, Y. Xiang, S. Vijayan, G. Li, Y. Huang, G. Cao, Y. Yang and H. Zhang, *Energy Storage Mater.*, 2018, **11**, 191–196.
38 J. Xu, Y. Chang, Y. Zhang, S. Ma, Y. Qu and C. Xu, *Appl. Surf. Sci.*, 2008, **255**, 1996–1999.
39 H. T. Cao, Z. L. Pei, J. Gong, C. Sun, R. F. Huang and L. S. Wen, *J. Solid State Chem.*, 2004, **177**, 1480–1487.
40 R. Zhang, X. R. Chen, X. Chen, X. B. Cheng, X. Q. Zhang, C. Yan and Q. Zhang, *Angew. Chem., Int. Ed.*, 2017, **56**, 7764–7768.